

Biomimetic Hierarchical Assembly of Helical Supraparticles from Chiral Nanoparticles

Yunlong Zhou,^{†,‡} Ryan L. Marson,^{§,||} Greg van Anders,^{†,§} Jian Zhu,[†] Guanxiang Ma,[†] Peter Ercius,[#] Kai Sun,^{||} Bongjun Yeom,^{†,¶} Sharon C. Glotzer,^{*,†,§,||} and Nicholas A. Kotov^{*,†,§,||,⊥}

[†]Department of Chemical Engineering, [§]Biointerfaces Institute, ^{||}Department of Materials Science and Engineering, [⊥]Department of Biomedical Engineering, University of Michigan, Ann Arbor, Michigan 48109, United States

[‡]Wenzhou Institute of Biomaterials and Engineering, CNITECH.CAS-Wenzhou Medical University, Wenzhou, Zhejiang 325011, People's Republic of China

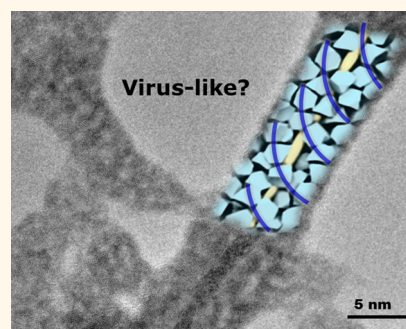
[#]National Center for Electron Microscopy, the Molecular Foundry, Lawrence Berkeley National Laboratory, Berkeley, California 94720, United States

[¶]Department of Chemical Engineering, Myongji University, Yongin, Gyeonggi-do 17058, South Korea

Supporting Information

ABSTRACT: Chiroptical materials found in butterflies, beetles, stomatopod crustaceans, and other creatures are attributed to biocomposites with helical motifs and multiscale hierarchical organization. These structurally sophisticated materials self-assemble from primitive nanoscale building blocks, a process that is simpler and more energy efficient than many top-down methods currently used to produce similarly sized three-dimensional materials. Here, we report that molecular-scale chirality of a CdTe nanoparticle surface can be translated to nanoscale helical assemblies, leading to chiroptical activity in the visible electromagnetic range. Chiral CdTe nanoparticles coated with cysteine self-organize around Te cores to produce helical supraparticles. D-/L-Form of the amino acid determines the dominant left/right helicity of the supraparticles. Coarse-grained molecular dynamics simulations with a helical pair-potential confirm the assembly mechanism and the origin of its enantioselectivity, providing a framework for engineering three-dimensional chiral materials by self-assembly. The helical supraparticles further self-organize into lamellar crystals with liquid crystalline order, demonstrating the possibility of hierarchical organization and with multiple structural motifs and length scales determined by molecular-scale asymmetry of nanoparticle interactions.

KEYWORDS: biomimetic nanoparticles, self-assembly, chirality, supraparticles, helices, virus-like nanostructures



Examples of astounding structural complexity of nature's materials raise the challenges of translating biological mechanisms of their synthesis to the industrial scale.^{1–4}

Inorganic nanoscale components are particularly attractive for many emerging and established technologies due to their special optical and electronic properties and their greater environmental robustness compared to many organic molecules.^{4–6}

Nature's method to fabricate and diversify its materials is based on the structural hierarchy utilizing a spectrum of small structural units that hierarchically self-organize across multiple scales into ever more sophisticated systems that can be in some cases replicated with man-made nanoscale materials.^{7,8} Therefore, one can ask a question: *Can the assembly of small inorganic building blocks with some biomimetic characteristics self-organize into hierarchical systems with a degree of complexity rivaling that found in nature?* Answer to this question will also help us understand better the limits of analogies between nanoparticles

and compact biomolecules with similar dimensions, such as proteins.⁴

Inorganic nanoparticles modified with an amino acid represent one of the simplest biomimetic inorganic building blocks.^{9–12} Notably, such particles can also be chiral; that is, their mirror image would not be superimposable with the original.¹³ Chirality is ubiquitous in living systems and important in virtually all biological functions.¹⁴ Its role in structural diversification can also be seen in the rapidly expanding spectrum of chiral metal and semiconductor nanomaterials with multiple functionalities.^{15–17} Also important, mathematical relationships between the symmetries of structural units and assemblies as well as their optical

Received: September 22, 2015

Accepted: February 22, 2016

Published: February 22, 2016

manifestations can complement the experimental discovery tools available for evaluation of assembly mechanisms.^{18–22}

RESULTS AND DISCUSSION

Here, we systematically investigate the self-organization of CdTe nanoparticles (NPs) modified with *L*- or *D*-cysteine (CYS) as the basic biomimetic building block. Despite a seemingly small difference in the energy of interactions associated with chiral asymmetry,²³ it was found that these NPs assemble into helical supraparticles with enantiomeric preference.

D- and *L*-CYS-stabilized CdTe NPs (denoted as *D*-NPs and *L*-NPs, respectively) were synthesized by the arrested precipitation method following a standard protocol (see Methods).²⁴ Note that notation *D* and *L* with respect to NPs denotes only the method of synthesis but not the chiral symmetry of the particles. Tetrahedral CdTe NPs could have symmetry that is similar to chiral *D* or *L* centers in amino acids when all the four corners have different truncations.²⁵ Alternatively, the atoms in the apexes of the NPs could also follow the familiar chiral pattern of tetrahedra with four different substituents.²⁶ In this work, however, we study the effect of chiral surface ligands on the surfaces of the four sides of tetrahedral NPs.

To observe self-organization, the CdTe NPs were precipitated by addition of 2-propanol and centrifuged for 5 min, followed by redispersion in deionized water with pH 9.0 in a nitrogen atmosphere (see Methods). The solution of NPs changed color from orange to dark red when left in the dark at room temperature for 8 h, indicating that self-assembly of NPs has occurred. It should be noted that the assembly conditions here are different from previous studies, in which the self-assembly was induced by light or different inter-particle forces.^{27–30} The conditions here enable the self-limiting assembly at the NP–NP interfaces capped with CYS surface ligands. The assembly process of CYS-stabilized NPs described here was critically influenced by the efficiency of oxygen removal and control over pH value, which are both key factors for successful helical assembly controlled by small anisotropy in NP interactions. When the assembly process was carried out under a high value of pH, *i.e.*, pH 11.0, the final assemblies displayed a morphology of dense NP chains irregularly attached on the surface of Te nanowires. If assembly occurred in an open atmosphere, NPs transitioned to a deeper oxidation state, a greater number of Te nanowires formed, and only a few NPs remained to assemble around them (Figure S1).

Scanning electron microscopy (SEM) showed the formation of nanorods (NRs) as the primary product of the self-assembly process. The lengths of the NRs were ~ 250 nm for assembly of *D*-NPs and ~ 300 nm for *L*-NPs (Figure 1a,b). The length of NRs can be controlled by the assembly conditions and can be as long as 5 μm using NPs synthesized with a molar ratio of CYS/Cd of 1.7:1 in a pH 10.0 solution, indicated in Figure 1c,d. The diameters of NRs assembled from *D*- and *L*-NPs are ~ 20 and ~ 23 nm, respectively, and reveal high uniformity. Both *D*- and *L*-NRs self-organize into even higher order lamellar assemblies. Similarly to liquid crystals, the self-organized structures from chiral NRs may also reveal a chiral, for instance, cholesteric, pattern of three-dimensional organization. Figure 1a and b, however, display only a two-dimensional representation of the higher order structures from NRs and are not sufficient to elaborate on the micrometer-scale chirality of the lamellae or potential twist in the mutual orientation of adjacent NRs.

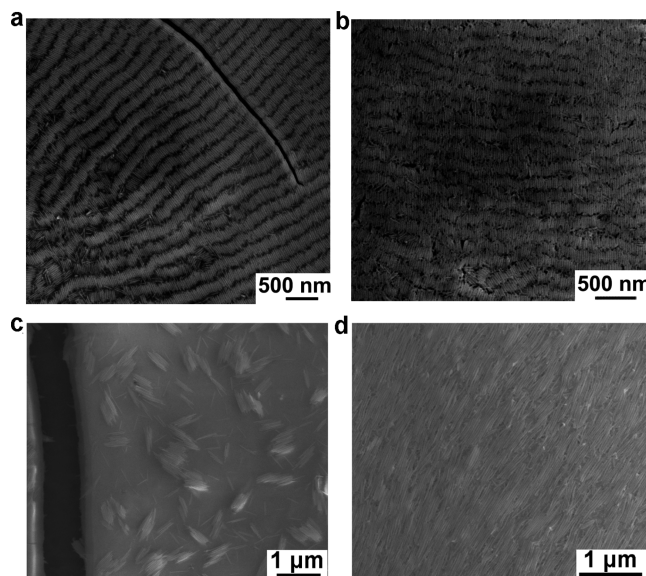


Figure 1. SEM images of NP assemblies from *D*-NPs (a, c) and *L*-NPs (b, d).

Scanning transmission electron microscopy (STEM) high angle annular dark-field (HAADF) images (Figure 2a,b,d, e) and STEM tomography (Figure 2c,f) showed that NRs have pronounced twist although not as regular as in DNA or some viruses.^{6,31} Comparing the organization of the biological and NP systems, we note that the outer shell of viruses also reveals a considerable amount of disorder and may not be perfectly packed especially under room-temperature imaging conditions. On the other hand, the size/shape distribution of NPs does decrease the perfection in the NR packing. Importantly, the self-assembly of NRs is enantioselective, with the twist directions dictated by the starting NPs' chirality. The NRs from *D*-NPs are *left*-handed, whereas those from *L*-NPs are *right*-handed helices that are easily distinguishable in tomographically reconstructed 3D images from tilt-series STEM–HAADF images (Figure 2c,f). AFM images also reveal their helical geometry in periodic topographical features typical for helices (Figure 2g,h). We evaluated the handedness of 100 samples by AFM images of helical NRs and found consistent dominance of a specific handedness of the helices. The overall yield of left-handed and right-handed helices from *D*-NPs and *L*-NPs is $\sim 70\%$ and $\sim 74\%$, respectively. The average pitch of helices seen in the TEM images is ~ 10 nm, which is further confirmed by SAXS data, revealing distinct peaks for both *D*- and *L*-NRs with $q = 0.05\text{\AA}^{-1}$, characteristic of a repetitive structural distance of 12.6 nm (Figure S2).

Nanoscale X-ray energy dispersive spectroscopy (XEDS) (Figure 3a–c) showed a Te/Cd atomic ratio of $\sim 2:1$ in the central part of the chiral helical structures; however, the Te to Cd ratio converges to 1:1 for the outside layer. High-resolution TEM (HRTEM) images (Figure 3d,e, Figure S3) indicate the CdTe NPs reside on the outside of the helical NRs; the center part is a single crystal nanowire with a diameter of ~ 5 nm. The thickness of the twisted CdTe layer is about 10–15 nm. Electron diffraction for the helical NRs reveals the presence of two phases: cubic CdTe and hexagonal Te. The diffraction spots for the CdTe phase correspond to (111) ($d = 0.39$ nm), (220) ($d = 0.22$ nm), and (311) ($d = 0.19$ nm) lattice planes. The diffraction patterns for the central Te-rich part show the maxima from (101) ($d = 0.32$ nm), (012) ($d = 0.23$ nm), and

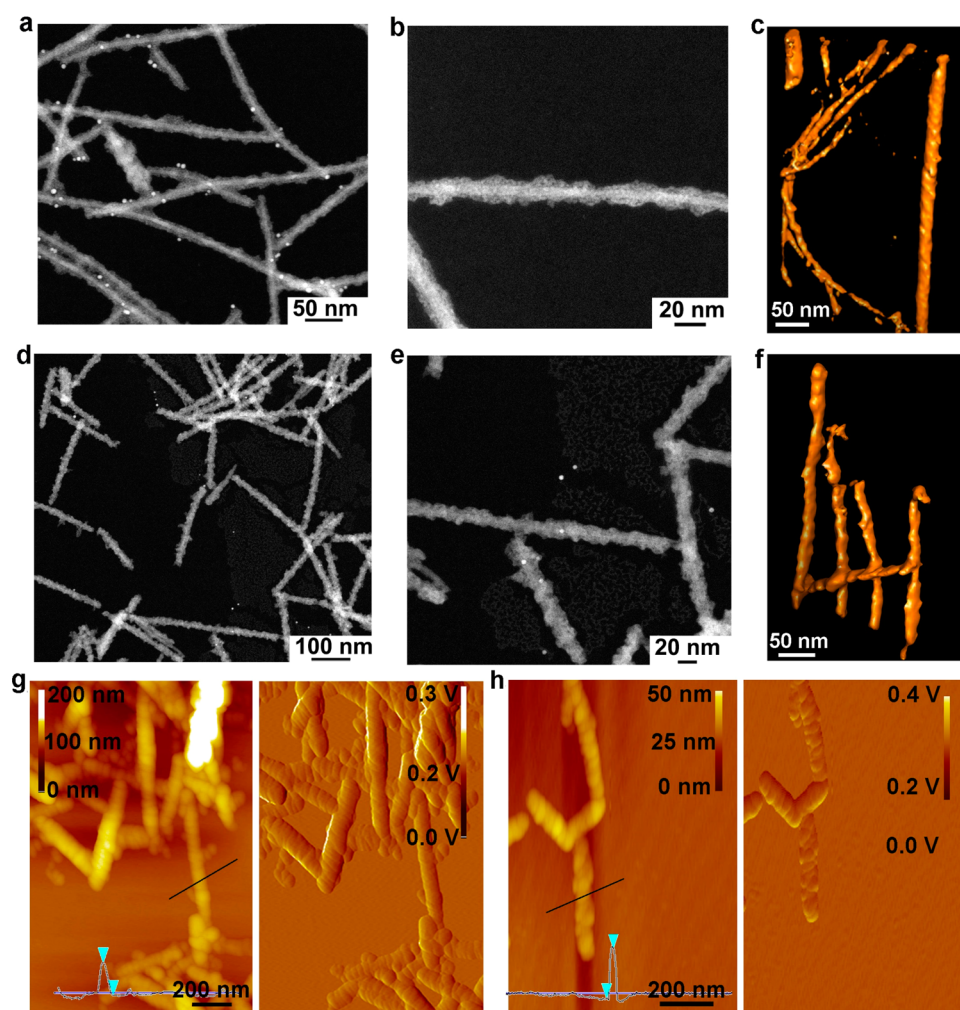


Figure 2. Nanoscale geometry of left- and right-handed helical NP assemblies. STEM–HAADF (a,b) and STEM (c) tomography images of left-NRs assembled from D-NPs. STEM–HAADF (d, e) and STEM (f) tomography images of right-NRs assembled from L-NPs. (g, h) AFM images of NRs obtained from D-NPs and L-NPs, left: height images, right: amplitude images. Note: In panels a, d, and e, the bright points are gold NPs added as markers for STEM tomography.

(110) ($d = 0.20$ nm) lattice planes. These data indicate that the helical NRs have unusually complex core–shell morphology, more sophisticated than what was observed before by Yeom *et al.*,²⁷ with a solid crystalline Te rod in the center and a polycrystalline NP shell on the outside. A gradual growth of the central ~ 5 nm Te rods/nanowires along the (001) direction is due to the slow oxidation process of CdTe (Figure 3a–f),³² and thus the control of the oxygen content in the media during the assembly is essential.

From the circular dichroism (CD) spectra (Figure 3h) one can see that the helical NRs have distinct chiroptical activity in the region from 300 to 800 nm, confirming enantioselectivity of the assembly process. Importantly, D- and L-NPs produce helical NRs with mirror-image CD spectra, whereas the precursors to the supraparticles, *i.e.*, NPs, and their early assemblies appearing as NP chains (Figure 4a, Figure S4) show no chiroptical activity in the visible range (Figure 3g). Only CD peaks associated with individual D- and L-CYS moieties in the UV spectral region between 200 and 300 nm appear.²⁴

To further understand the mechanism of the assembly process and the driving forces responsible for the enantioselective transition of D/L-NPs to NRs, we examined the dispersions using different spectroscopy and microscopy

techniques at the time points of 8, 24, 48, and 72 h (Figure 4, Figures S4–S8). In the first 8 h, TEM bright-field (BF) images revealed transformation of short NP chains for both enantiomers of CdTe particles (Figure 4, Figure S4). The L-NP assemblies show a broad and weak positive CD peak at ~ 430 nm compared with the NP solution and D-NP assemblies (Figure S6b,d). By 24 h, the chains transformed into short NRs that display chiroptical activity (Figure 4, Figure S6). Neither morphology nor CD spectra for mixed D/L-NP assemblies could show the same changes in 48 h. After 48 and 72 h, both D-NP and L-NP assemblies show self-organization into short helical rods, for which the corresponding CD spectra display peaks and Cotton effects of opposite signs (Figure S6).²⁴ Note that the intermediate stages *en route* from single NPs to helical NRs are markedly different from previous observations for assemblies of organic and inorganic helical systems.^{18,33–35} The growth of Te cores takes place concurrently with the attachment of CdTe, which presents, perhaps, another surprising parallel with biological self-assembled structures.

The zeta potential decreased with time for both D-NP and L-NP assemblies (Figure S7), indicating the continuously decreasing repulsive interactions between the NPs and the NRs. Such a temporal trend in ζ is conducive to the self-

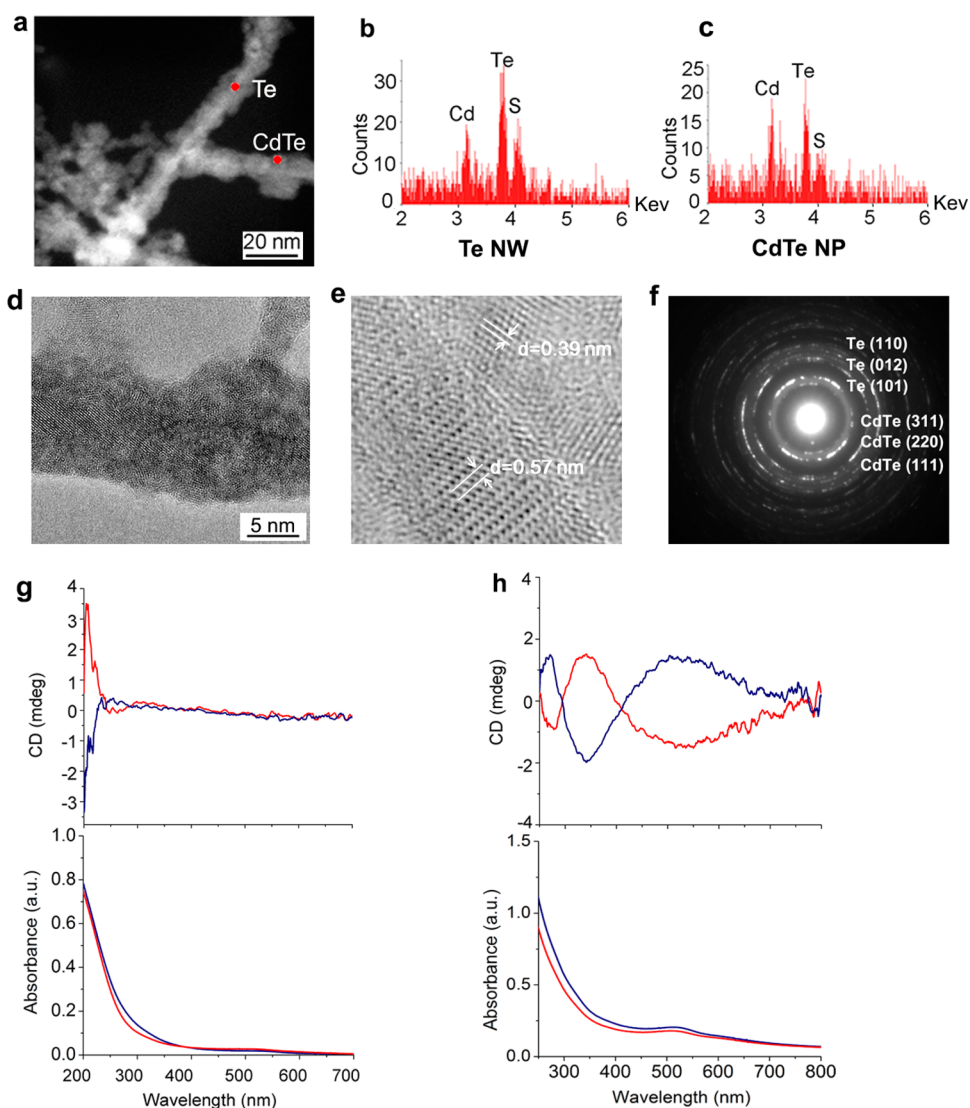


Figure 3. Nanoscale structure and chirality of helical NP assemblies. (a–c) XEDS analysis of peripheral and core parts of *left*-handed helical NRs. (d, e) HRTEM image of peripheral CdTe NPs and Te core. (f) Electron diffraction of the *right*-handed NRs. (g) CD/UV-vis spectra of supraparticle precursors: NP chains obtained after 8 h of assembly of D- (red) and L-NPs (blue). (h) CD spectra of *left*- (red) and *right*-handed (blue) helical NRs obtained after 2 weeks of assembly. Complementary CD/UV-vis spectra of L/D-cysteine are given in Figure S5.

limiting aggregation of NPs into supraparticles.^{36,37} The uniformity of NR diameters leading to their hierarchical organization into the lamellar phase (Figure 1a,b) is also indicative of the self-limiting terminal assembly pattern. Photoluminescence (PL) and UV-vis spectra remain essentially unchanged (Figures S8, Figure S6c,d); the red-shift of the luminescence due to aggregation is (over)compensated by the blue-shift due to oxidation, leading to the formation of Te cores. PL lifetimes increased from 22 ns for D-NPs to 52 ns for the left-handed helix and from 19 ns for L-NPs to 35 ns for the right-handed helix (Figure S9). There could be several reasons for such a noticeable change in PL dynamics. One of them is the decrease of the spatial confinement of the electrons and holes. Another could be the formation of a thin layer of CdS on the surface of CdTe NPs from the decomposition of cysteine surface ligands. The CdS layer can elongate the lifetime of the electron-hole pair by temporary localization of some of the charge carriers.^{38,39}

Previous reports indicated that the self-organization of helices from organic building blocks arises mainly from the

concerted action of multiple types of short-range and long-range interactions.³⁷ Hydrogen bonding and hydrophobic interactions are some of the most important forces in the self-organization of chiral biotic assemblies, e.g., the DNA double-helical structure and chiral peptides-amphiphile nanofibers.^{40,41} Biomolecule-stabilized inorganic NPs can interact *via* a similar set of intermolecular interactions as biological species of the same size, although the van der Waals attraction between them is typically stronger due to higher values of pairwise Hamaker constants.⁴² Therefore, we hypothesize that the formation of helical NRs is due to the chirality of interactions at the NP-NP interfaces capped with CYS moieties as opposed to chiral preference of the packing of NP cores,⁴³ NR twisting,⁴⁴ oriented attachment,⁴⁵ or screw axis dislocation.⁴⁶

Compared to other types of inter-NP interactions,⁴⁷ which include van der Waals forces, dipole-dipole, charge-charge, and charge-dipole interactions, hydrogen bonds, and other interactions between NPs, this chiral contribution may appear to be small, but it is actually appreciable, especially for chiral molecules on the surface of NPs. The energy difference

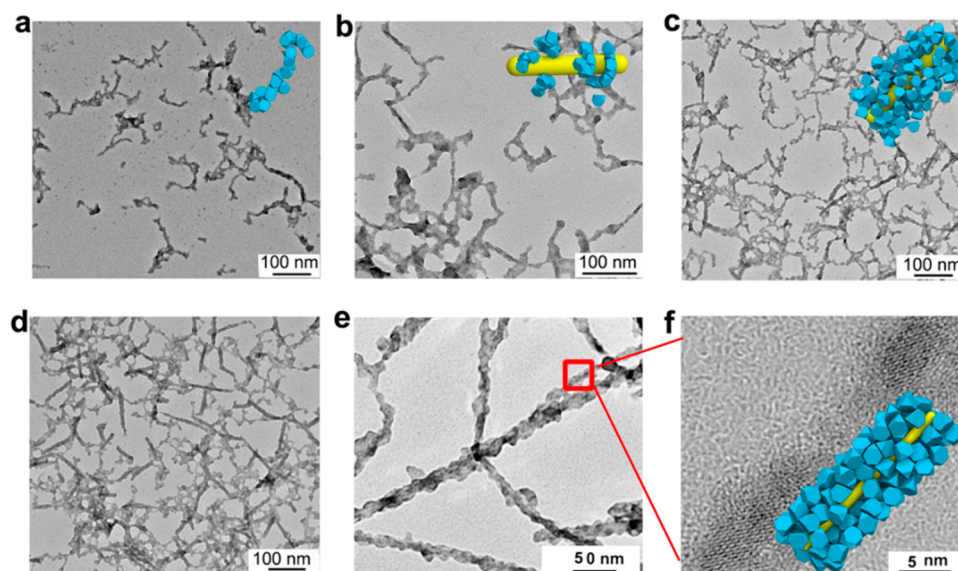


Figure 4. Intermediate stages of self-organization of helical hierarchical assemblies from D-NPs. (a–d) TEM BF images of the formation process of *left-handed* NRs by assembly of D-NPs in 8 h (a), 24 h (b), 48 h (c), and 72 h (d). TEM BF (e) and HREM (f) images of helical NRs obtained after 72 h of assembly. Inset images are the simulated assembly of helical NRs from a CdTe NP; the central Te core is yellow, and the surrounding CdTe NPs are blue.

between intermolecular bonds binding two homochiral CYS molecules or two heterochiral CYS molecules is comparable to other forces. According to Kühnle *et al.*, the heterochiral dimer of gold-bound CYS was found to be energetically less favorable than the homochiral dimers by *ca.* 0.2 eV, *i.e.*, 20 kJ/mol at 295 K.²³ The three-point bonding involving carboxyl groups and amine–gold interactions give an LL pair advantage over an LD pair. CYS molecules in our system are bound to the surface of CdTe, and the same three-point intermolecular interactions involving the carboxylic group and amino group coordination to the cadmium atoms on the CdTe surface are likely to take place.⁴⁸ The energy cost for breaking the cysteine–Cd²⁺ tetrahedral coordination bond affected by the rotation of the amino acid segments and/or its chirality can be as high as 117.3 kcal/mol (490.8 kJ/mol);⁴⁹ thus its deformation depending on the even seemingly minor alteration of the atomic structures can easily amount to 20 kJ/mol.

For comparison, the energy of dipolar attraction, known to be a significant factor determining the geometry of self-assembled structures for 3.2 nm CdTe NPs, can be estimated to be *ca.* 9.7 kJ/mol using, for instance, the classical formula for aligned dipoles (Supporting Information, Part I).³⁰ This juxtaposition with dipole–dipole interactions shows the importance of the chiral interactions as a determinant of the assembly geometry, especially considering their cooperative nature of ligand-to-ligand interactions for the face-to-face contact between NPs.

To confirm that the molecular-scale chirality of CYS surface ligands can indeed translate into the nanoscale chirality of the NRs, we performed coarse-grained molecular dynamics (MD) simulations of NP self-assembly (Supporting Information Part II). Four primary features of the experimental system, *i.e.*, the excluded volume effects due to the NP shape, the attraction of the NPs to the surface of the Te core, dipolar interactions, and the chiral asymmetry of NP–NP interactions originating from the CYS layer on the NP surface (Figure 5a), included in the simulations. Among others, excluded volume effects are captured *via* a purely repulsive Weeks–Chandler–Andersen

potential from the NP surface.⁵⁰ To model the axial form of the Te core, we confine particles using a cylindrical harmonic well $U = \frac{1}{2}kx^2$ (where x denotes the radial distance from the z -axis) at the center of the simulation box. To account for the twisting preference induced by the amino acid surface ligand, we include a specially developed chiral potential that acts between interacting faces of the particles. The potential describes the cumulative torque from collective interactions of chiral surface ligands on the NP surfaces; it changes signs for the clockwise and counterclockwise direction of rotation, as can be seen in the description of the potential with respect to face normals given in the SI (Figure S12). For the entire NP the total energy of chiral interactions affecting its motion in the simulations was ± 1 , 10, and 100 $k_B T$ (0.41, 4.1, and 41.0 kJ/mol at 295 K), the lower values of which are an underestimate considering the 20 kJ/mol at 295 K difference stemming from the chiral asymmetry of CYS.²³

Simulated assemblies without the D/L asymmetry of CYS–CYS interactions resulted in chiral structures, but without preferred handedness. The chirality of these terminal assemblies is the result of the confinement of multiparticle assemblies to a cylindrical surface. The pitch and geometry of such structures can be described analytically and strongly depend on the ratio of diameters between the NP and the structure-directing cylinder.⁵¹ In contrast, when we included the chiral interaction between NPs, the assembly of the supraparticular NRs was enantioselective for interaction energies of 10 $k_B T$ (4.1 kJ/mol) and above (Figure 5b,c). This value is noticeably smaller than the estimated 20 kJ/mol energy difference for surface–bound homo- and heterochiral CYS dimers made above. Multiple and cooperative CYS–CYS interactions can occur for face-to-face contacts between tetrahedral NPs, thereby further increasing the energy preference and enantiomeric bias.

Structures with predictable chirality were observed in simulations of particles between 100 and 300 particles and for rod diameters of 1 and 2 NP widths; the effects are

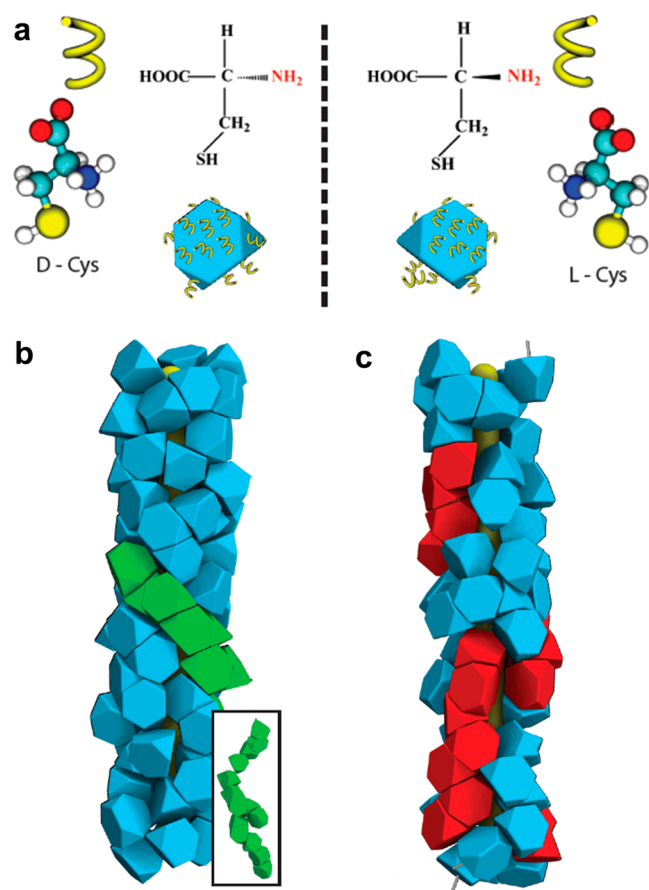


Figure 5. Simulated helical hierarchical assemblies of D- and L-NPs. (a) Schematics of the NP surfaces coated with D- and L-CYS. Chemical structures are related to a “steric coil”. Structures produce a predetermined twist based upon the chirality of the stabilizer by biasing local NP motifs. Either *left* (b) or *right* (c) handed structures are produced, depending upon the choice of “twist”, as determined by a chiral interaction between NP faces. The Te core is shown in yellow, with an outer layer of NPs removed. Insets show the unaltered wire (top) and centers of mass of the NPs connected with bonds along closest neighbors (bottom).

particularly pronounced in simulations where the particle number, rod thickness, and box length were commensurate with a close packing of tetrahedra around the rod.

The data described so far show that molecular chirality of stabilizers induces the formation of chiral superstructures. To confirm the finding that molecular-scale chirality is reflected in the nanoscale geometry of the assemblies, we also need to test the case of racemic stabilizer-capped NPs. Therefore, we carried out a complementary experimental and computational study of self-assembly processes from *rac*-NPs taken in the same amount and assembled under the same conditions. The *in-silico* assemblies driven by an achiral interparticle pair-potential demonstrated (Figure 6f) no distinct handedness, as opposed to the helical assemblies in Figure 5b,c. Concomitant TEM and AFM results of the experimental supraparticle NRs made from *rac*-NPs show intertwined rod-like assemblies with a diameter of ~ 40 nm, which is almost double the diameter (Figure 6 and Figure S10a) of helical NRs in Figure 1. The experimental terminal assemblies of *rac*-NPs are composed of many intertwined thin, ~ 2 nm nanowires attached with CdTe NPs according to HRTEM image and XEDS analysis (Figure 6c, Figure S11), in which the presence of the hexagonal Te phase

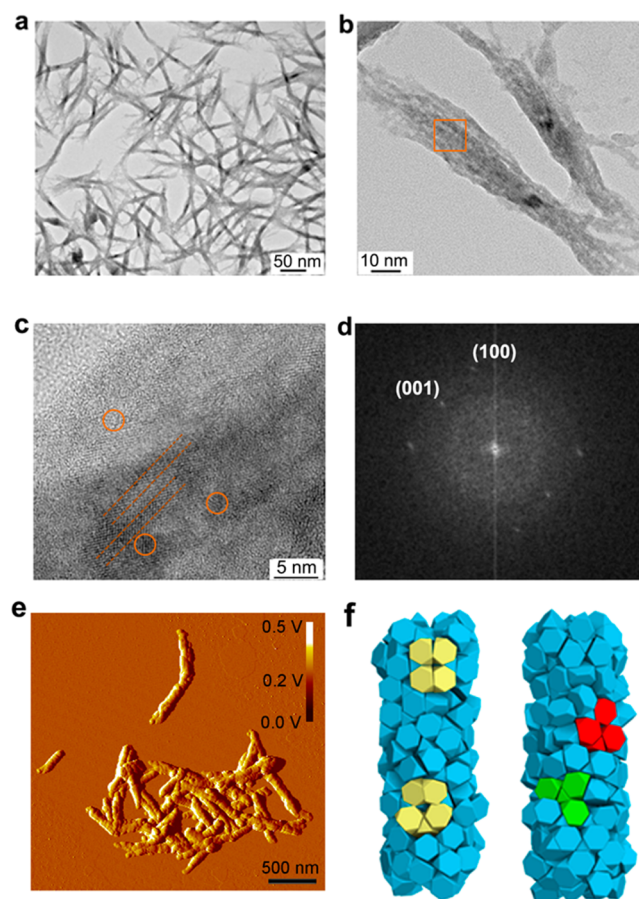


Figure 6. Supraparticle NRs resulting from self-assembly of *rac*-NPs. (a, b) TEM BF images of the NR formed from the *rac*-NPs. HRTEM (c) and its corresponding FFT pattern (d) characterizations of twinning structures of Te attached with CdTe NPs and corresponding fast Fourier transform pattern of Te nanowires. The fast Fourier transform pattern of the hexagonal Te phase corresponds to (100) (0.38 nm) and (001) (0.6 nm).³² (e) AFM amplitude image of self-assembled supraparticle NRs from *rac*-NPs. (f) Simulations of assemblies of tetrahedral *rac*-NPs (left: front, right: back).

can be discerned from the fast Fourier transform pattern (Figure 6d). CD spectra show a weak band around 350–550 nm, which may be surprising (Figure S10b). This CD band observed for *rac*-NP assemblies is broader than the CD bands obtained for NPs with homochiral surface ligands. At the same time, we see no evidence of helical or other assemblies of NPs with specific chiral preference in TEM and AFM data. The small chiral bias visible in CD spectroscopy for NP mixtures with expected racemic behavior (although they might not be truly racemic) can be attributed to stochastically assembled small NP clusters and should be investigated further.

CONCLUSIONS

Overall, our findings in this study demonstrate that a small biomimetic unit can drive hierarchical self-assemblies across several scales. The self-assembly of NPs with atomic-scale chirality imparted by the surface ligands results in the formation of helical supraparticles structurally resembling biological prototypes exemplified by the tobacco mosaic virus. The nanoscale twists of helical supraparticles are deterministically controlled by the molecular-scale chirality of the constitutive

NPs, which lays the groundwork for understanding the collective behavior of nanoscale biomimetic units. The resulting helical NRs can further self-organize into lamellar liquid crystals, which expand the family of hierarchical assemblies of anisotropic inorganic particles.^{27,37} Although possible, chiral order in the lamellar assemblies at the micrometer scale was not observed in this work, and further studies regarding potential chiral hierarchy in these superstructures need to be undertaken. The self-assembly phenomena reported here present multiple venues for further research toward biologically inspired assembly processes, chiral catalysis, drug delivery, and polarization-based optoelectronic technologies.^{52–57}

MATERIALS AND METHODS

Materials. Cadmium perchlorate hexahydrate was purchased from Alfa-Aesar. Aluminum telluride powder was purchased from Materion Advanced Chemicals. L-cysteine (L-CYS) hydrochloride and D-cysteine (D-CYS) hydrochloride were purchased from Sigma-Aldrich. All chemicals are used as received.

Synthesis and Assembly of (D, L, and rac)-cysteine-Stabilized CdTe NPs (D-NPs, L-NPs, and rac-NPs). The molar ratio of CYS to Cd²⁺ used in the synthesis of the NPs was 2.2:1, and the synthesis concentration of Cd²⁺ was 0.01 mol/L. In order to reduce the possibility of decomposition of cysteine in highly basic solutions, the solution of cadmium perchlorate and cysteine was taken at pH 9.6. We briefly dissolved 0.373 g of cadmium perchlorate hexahydrate and 0.343 g of D-CYS, L-CYS, or rac-CYS in 80 mL of 18 MΩ pure water, subsequently adjusting the pH value to 9.6. The solution was purged with nitrogen for 1.0 h to remove oxygen. CdTe NPs nucleate after subsequent purging of H₂Te generated separately by mixing 0.5 M H₂SO₄ and 0.08 g of Al₂Te₃. The CdTe NPs' growth was conducted at 90 °C for 4 h and then cooling to room temperature with nitrogen bubbling. The assembly procedure can be summarized as followed: We added a 1:1 volume ratio of 2-propanol to the freshly prepared CdTe solution and centrifuged the mixture solution at 6000 rpm/min for 10 min. After removing the supernatant containing free cadmium complexes and other salts, we immediately dissolved CdTe in pH 9.0 ultrapure water and bubbled with nitrogen for 5 min. Solutions were kept in 20 mL glass vials sealed with Parafilm at room temperature. It can be found that the solution of nanoparticles changes in color from orange to dark red when left in a dark place at room temperature for 8 h, giving a visual indication that the self-assembly of NPs has occurred.

Characterization. Samples for characterizations were first centrifuged at 5000 rpm/min for 5 min, and then the precipitates were redispersed in water in order to remove the random network assemblies in the precursors. In order to get the real-time morphology in the process of self-assembly, the CD spectra and other data about intermediate states were obtained with samples without separation of NP chains and supraparticles NRs. Circular dichroism spectra were collected on a JASCO-815. Fluorescence spectra were carried on a Horiba Fluoro MAX-3. AFM images were taken using the tapping model on a Bruker Multimode-II. TEM images were taken by a JEM-3011 transmission electron microscope. Annular dark-field STEM images and XEDS analysis were taken using a JEOL 2010F scanning transmission electron microscope at 200 kV. SEM images were conducted on a FEI Nova NanoLab scanning electron microscope. STEM tomography images were collected on a FEI Titan in annular dark-field mode at 200 kV at the Molecular Foundry, Lawrence Berkeley National Lab. The collection angle was from -70° to +70°. Tomographic alignment of a tilt series and 3D reconstruction were performed using IMOD software. This is achieved by first tracking the small movement of fiducial gold markers with a diameter of 10 nm. Then, the reconstructed volume was filtered using a Gaussian (width, 1) for noise reduction in UCSF Chimera software. SAXS were conducted on a Bruker NanoStar small-angle X-ray scattering (SAXS) system.

ASSOCIATED CONTENT

Supporting Information

The Supporting Information is available free of charge on the ACS Publications website at DOI: 10.1021/acsnano.5b05983.

Addition electron microscopy images, optical characterizations, zeta potential, SAXS data, and simulations (PDF)

AUTHOR INFORMATION

Corresponding Authors

*E-mail: sglotzer@umich.edu.

*E-mail: kotov@umich.edu.

Notes

The authors declare no competing financial interest.

ACKNOWLEDGMENTS

This material is based upon work supported by the U.S. Army Research Office under Grant Award No. ARO MURI W911NF-10-1-0518. Y.L.Z. acknowledges support from National Natural Science Foundation of China (NSFC-21573162) and WIBEZD2014001-02. R.L.M. and N.A.K. were supported in part by the National Science Foundation, Division of Materials Research Award # DMR 1120923. N.A.K. also wishes to acknowledge support from NSF under grants ECS-0601345; CBET 0933384; CBET 0932823; and CBET 1036672. We thank the University of Michigan's Electron Microscopy and Analysis Laboratory (EMAL) for its assistance with electron microscopy and for NSF grants (numbers DMR-0320740 and DMR-9871177), for funding the FEI Nova Nanolab Dualbeam focused ion beam workstation and scanning electron microscope and the JEM-2010F analytical electron microscope used in this work. Y.L.Z. thanks Jinyan Chen and Hailin Qiu for the assistance with the PL lifetime experiment. R.L.M. is grateful to Matthew Spellings for numerous fruitful discussions. Simulations were carried out using computational resources and services supported by Advanced Research Computing at the University of Michigan, Ann Arbor. The experiments performed at the Molecular Foundry, Lawrence Berkeley National Laboratory were supported by the U.S. Department of Energy under contract no. DE-AC02-05CH11231. We also thank EMAL and the College of Engineering for assistance with the Bruker NanoStar small-angle X-ray scattering. The experiments performed at the Molecular Foundry, Lawrence Berkeley National Laboratory were supported by the U.S. Department of Energy under contract #DE-AC02-05CH11231.

REFERENCES

- (1) Vukusic, P.; Sambles, J. R. Photonic Structures in Biology. *Nature* **2003**, *424*, 852–855.
- (2) Shopsowitz, K. E.; Qi, H.; Hamad, W. Y.; MacLachlan, M. J. Free-Standing Mesoporous Silica Films with Tunable Chiral Nematic Structures. *Nature* **2010**, *468*, 422–425.
- (3) Whitesides, G. M.; Grzybowski, B. Self-Assembly at All Scales. *Science* **2002**, *295*, 2418–2421.
- (4) Kotov, N. A. Inorganic Nanoparticles as Protein Mimics. *Science* **2010**, *330* (6001), 188–189.
- (5) Liu, S. H.; Han, L.; Duan, Y. Y.; Asahina, S.; Terasaki, O.; Cao, Y. Y.; Liu, B.; Ma, L. G.; Zhang, J. L.; Che, S. A. Synthesis of Chiral TiO₂ Nanofibre with Electron Transition-Based Optical Activity. *Nat. Commun.* **2012**, *3*, 1215.
- (6) Kim, J.-Y.; Kotov, N. A. Charge Transport Dilemma of Solution-Processed Nanomaterials. *Chem. Mater.* **2014**, *26* (1), 134–152.

- (7) Aggeli, A.; Nyrkova, I. A.; Bell, M.; Harding, R.; Carrick, L.; McLeish, T. C. B.; Semenov, A. N.; Boden, N. Hierarchical Self-Assembly of Chiral Rod-Like Molecules as a Model for Peptide β -sheet Tapes, Ribbons, Fibrils, and Fibers. *Proc. Natl. Acad. Sci. U. S. A.* **2001**, *98*, 11857–11862.
- (8) Querejeta-Fernández, A.; Hernández-Garrido, J. C.; Yang, H.; Zhou, Y.; Green, P. F.; Varela, A.; Parras, M.; Calvino-Gómez, J. J.; González-Calbet, J. M.; Kotov, N. A. Unknown Aspects of Self-Assembly of PbS Microscale Superstructures. *ACS Nano* **2012**, *6* (5), 3800–3812.
- (9) Schaaff, T. G.; Knight, G.; Shafiqullin, M. N.; Borkman, R. F.; Whetten, R. L. Isolation and Selected Properties of a 10.4 kDa Gold:Glutathione Cluster Compound. *J. Phys. Chem. B* **1998**, *102*, 10643–10646.
- (10) Govorov, A. O.; Gun'ko, Y. K.; Slocik, J. M.; Gerard, V. A.; Fan, Z.; Naik, R. R. Chiral Nanoparticle Assemblies: Circular Dichroism, Plasmonic Interactions, and Exciton Effects. *J. Mater. Chem.* **2011**, *21*, 16806–16818.
- (11) Gautier, C.; Burgi, T. Vibrational Circular Dichroism of N-acetyl-L-cysteine Protected Gold Nanoparticles. *Chem. Commun.* **2005**, *43*, 5393–5395.
- (12) Jadzinsky, P. D.; Calero, G.; Ackerson, C. J.; Bushnell, D. A.; Kornberg, R. D. Structure of a Thiol Monolayer-Protected Gold Nanoparticle at 1.1 Å Resolution. *Science* **2007**, *318*, 430–433.
- (13) Liu, Y. M.; Zhang, X. Metamaterials: A New Frontier of Science and Technology. *Chem. Soc. Rev.* **2011**, *40*, 2494–2507.
- (14) Zhang, M. X.; Qing, G. Y.; Sun, T. L. Chiral Biointerface Materials. *Chem. Soc. Rev.* **2012**, *41*, 1972–1984.
- (15) Shemer, G.; Krichevski, O.; Markovich, G.; Molotsky, T.; Lubitz, I.; Kotlyar, A. B. Chirality of Silver Nanoparticles Synthesized on DNA. *J. Am. Chem. Soc.* **2006**, *128*, 11006–11007.
- (16) Moloney, M. P.; Gun'ko, Y. K.; Kelly, J. M. Chiral Highly Luminescent CdS Quantum Dots. *Chem. Commun.* **2007**, *38*, 3900–3902.
- (17) Garzón, I.; Beltrán, M.; González, G.; Gutierrez-González, I.; Michaelian, K.; Reyes-Nava, J.; Rodríguez-Hernández, J. Chirality, Defects, and Disorder in Gold Clusters. *Eur. Phys. J. D* **2003**, *24*, 105–109.
- (18) Song, C. Y.; Blaber, M. G.; Zhao, G. P.; Zhang, P. J.; Fry, H. C.; Schatz, G. C.; Rosi, N. L. Tailorable Plasmonic Circular Dichroism Properties of Helical Nanoparticle Superstructures. *Nano Lett.* **2013**, *13*, 3256–3261.
- (19) Hendry, E.; Carpy, T.; Johnston, J.; Popland, M.; Mikhaylovskiy, R. V.; Laphorn, A. J.; Kelly, S. M.; Barron, L. D.; Gadegaard, N.; Kadodwala, M. Ultrasensitive Detection and Characterization of Biomolecules using Superchiral Fields. *Nat. Nanotechnol.* **2010**, *5*, 783–787.
- (20) Hentschel, M.; Schaferling, M.; Weiss, T.; Liu, N.; Giessen, H. Three-Dimensional Chiral Plasmonic Oligomers. *Nano Lett.* **2012**, *12*, 2542–2547.
- (21) Guerrero-Martínez, A.; Alonso-Gómez, J. L.; Auguie, B.; Cid, M. M.; Liz-Marzán, L. M. From Individual to Collective chirality in Metal Nanoparticles. *Nano Today* **2011**, *6*, 381.
- (22) Baimuratov, A. S.; Rukhlenko, I. D.; Gun'ko, Y. K.; Baranov, A. V.; Fedorov, A. V. Dislocation-Induced Chirality of Semiconductor Nanocrystals. *Nano Lett.* **2015**, *15*, 1710–1715.
- (23) Kuhnle, A.; Linderoth, T. R.; Hammer, B.; Besenbacher, F. Chiral Recognition in Dimerization of Adsorbed Cysteine Observed by Scanning Tunneling Microscopy. *Nature* **2002**, *415*, 891–893.
- (24) Zhou, Y. L.; Zhu, Z. N.; Huang, W. X.; Liu, W. J.; Wu, S. J.; Liu, X. F.; Gao, Y.; Zhang, W.; Tang, Z. Y. Optical Coupling Between Chiral Biomolecules and Semiconductor Nanoparticles: Size-Dependent Circular Dichroism Absorption. *Angew. Chem., Int. Ed.* **2011**, *50*, 11456–11459.
- (25) Yan, W. J.; Xu, L. G.; Xu, C. L.; Ma, W.; Kuang, H.; Wang, L. B.; Kotov, N. A. Self-Assembly of Chiral Nanoparticle Pyramids with Strong R/S Optical Activity. *J. Am. Chem. Soc.* **2012**, *134*, 15114–15121.
- (26) Zhou, Y. L.; Yang, M.; Sun, K.; Tang, Z. Y.; Kotov, N. A. Similar Topological Origin of Chiral Centers in Organic and Nanoscale Inorganic Structures: Effect of Stabilizer Chirality on Optical Isomerism and Growth of CdTe Nanocrystals. *J. Am. Chem. Soc.* **2010**, *132*, 6006–6013.
- (27) Yeom, J.; Yeom, B.; Chan, H.; Smith, K. W.; Dominguez-Medina, S.; Bahng, Joong, H.; Zhao, G. P.; Chang, W.-S.; Chang, S.-J.; Chuvin, A.; Melnikau, D.; Rogach, A. L.; Zhang, P. J.; Link, S.; Král, P.; Kotov, N. A. Chiral Templating of Self-Assembling Nanostructures by Circularly Polarized Light. *Nat. Mater.* **2015**, *14*, 66–72.
- (28) Hu, T.; Isaacoff, B. P.; Bahng, J. H.; Hao, C. L.; Zhou, Y. L.; Zhu, J.; Li, X. Y.; Wang, Z. L.; Liu, S. Q.; Xu, C. L.; Biteen, J. S.; Kotov, N. A. Self-Organization of Plasmonic and Excitonic Nanoparticles into Resonant Chiral Supraparticle Assemblies. *Nano Lett.* **2014**, *14*, 6799–6810.
- (29) Srivastava, S.; Santos, A.; Critchley, K.; Kim, K.-S.; Podsiadlo, P.; Sun, K.; Lee, J.; Xu, C. L.; Lilly, G. D.; Glotzer, S. C.; Kotov, N. A. Light-Controlled Self-Assembly of Semiconductor Nanoparticles into Twisted Ribbons. *Science* **2010**, *327*, 1355–1359.
- (30) Tang, Z. Y.; Kotov, N. A.; Giersig, M. Spontaneous Organization of Single CdTe Nanoparticles into Luminescent Nanowires. *Science* **2002**, *297*, 237–240.
- (31) Klug, A. The Tobacco Mosaic Virus Particle: Structure and Assembly. *Philos. Trans. R. Soc., B* **1999**, *354*, 531–535.
- (32) Tang, Z. Y.; Wang, Y.; Sun, K.; Kotov, N. A. Spontaneous Transformation of Stabilizer-Depleted Binary Semiconductor Nanoparticles into Selenium and Tellurium Nanowires. *Adv. Mater.* **2005**, *17*, 358–363.
- (33) Prins, L. J.; Huskens, J.; de Jong, F.; Timmerman, P.; Reinhoudt, D. N. Complete Asymmetric Induction of Supramolecular Chirality in A Hydrogen-Bonded Assembly. *Nature* **1999**, *398*, 498–502.
- (34) Bierman, M. J.; Lau, Y. K. A.; Kvit, A. V.; Schmitt, A. L.; Jin, S. Dislocation-Driven Nanowire Growth and Eshelby Twist. *Science* **2008**, *320*, 1060–1063.
- (35) Govorov, A. O.; Gun'ko, Y. K.; Slocik, J. M.; Gerard, V. A.; Fan, Z.; Naik, R. R. Chiral Nanoparticle Assemblies: Circular Dichroism, Plasmonic Interactions, and Exciton Effects. *J. Mater. Chem.* **2011**, *21*, 16806–16818.
- (36) Xia, Y. S.; Nguyen, T. D.; Yang, M.; Lee, B.; Santos, A.; Podsiadlo, P.; Tang, Z. Y.; Glotzer, S. C.; Kotov, N. A. Self-assembly of Self-limiting Monodisperse Supraparticles from Polydisperse Nanoparticles. *Nat. Nanotechnol.* **2011**, *6*, 580–587.
- (37) Nguyen, T. D.; Schultz, B. A.; Kotov, N. A.; Glotzer, S. C. Generic, Phenomenological, On-The-Fly Renormalized Repulsion Model for Self-Limited Organization of Terminal Supraparticle Assemblies. *Proc. Natl. Acad. Sci. U. S. A.* **2015**, *112*, 3161–3168.
- (38) Dai, M.-Q.; Zheng, W.; Huang, Z.; Lanry Yung, L.-Y. Aqueous Phase Synthesis of Widely Tunable Photoluminescence Emission CdTe/CdS Core/Shell Quantum Dots under A Totally Ambient Atmosphere. *J. Mater. Chem.* **2012**, *22*, 16336–16345.
- (39) Zeng, Q. H.; Kong, X. G.; Sun, Y. J.; Zhang, Y. L.; Tu, L. P.; Zhao, J. L.; Zhang, H. Synthesis and Optical Properties of Type II CdTe/CdS Core/Shell Quantum Dots in Aqueous Solution *via* Successive Ion Layer Adsorption and Reaction. *J. Phys. Chem. C* **2008**, *112*, 8587–8593.
- (40) Paramonov, S. E.; Jun, H.-W.; Hartgerink, J. D. Self-Assembly of Peptide–Amphiphile Nanofibers: The Roles of Hydrogen Bonding and Amphiphilic Packing. *J. Am. Chem. Soc.* **2006**, *128*, 7291–7298.
- (41) Zhang, S. G. Fabrication of Novel Biomaterials Through Molecular Self-assembly. *Nat. Biotechnol.* **2003**, *21*, 1171–1178.
- (42) Kotov, N. A. *Terminal and Extended Assemblies of Nanoparticles*, MPL Lecture; California Institute of Technology, Pasadena, CA, March 26, 2014.
- (43) Damasceno, P. F.; Engel, M.; Glotzer, S. C. Predictive Self-Assembly of Polyhedra into Complex Structures. *Science* **2012**, *337*, 453–457.
- (44) Ma, W.; Kuang, H.; Wang, L. B.; Xu, L. G.; Chang, W.-S.; Zhang, H. N.; Sun, M. Z.; Zhu, Y. Y.; Zhao, Y.; Liu, L. Q.; Xu, C. L.;

Link, S.; Kotov, N. A. Chiral Plasmonics of Self-assembled Nanorod Dimers. *Sci. Rep.* **2013**, *3*, 1934.

(45) Cho, K.-S.; Talapin, D. V.; Gaschler, W.; Murray, C. B. Designing PbSe Nanowires and Nanorings Through Oriented Attachment of Nanoparticles. *J. Am. Chem. Soc.* **2005**, *127*, 7140–7147.

(46) Han, X. D.; Zhang, Y. F.; Zheng, K.; Zhang, X. N.; Zhang, Z.; Hao, Y. J.; Guo, X. Y.; Yuan, J.; Wang, Z. L. Low-Temperature *in situ* Large Strain Plasticity of Ceramic SiC Nanowires and Its Atomic-Scale Mechanism. *Nano Lett.* **2007**, *7*, 452–457.

(47) Bishop, K. J.; Wilmer, C. E.; Soh, S.; Grzybowski, B. A. Nanoscale Forces and Their Uses in Self-Assembly. *Small* **2009**, *5*, 1600–1630.

(48) Mah, V.; Jalilvand, F. Cadmium(II) Complex Formation with Glutathione. *J. Biol. Inorg. Chem.* **2010**, *15*, 441–458.

(49) Rulíšek, L.; Havlas, Z. Theoretical Studies of Metal Ion Selectivity. 1. DFT Calculations of Interaction Energies of Amino Acid Side Chains with Selected Transition Metal Ions (Co^{2+} , Ni^{2+} , Cu^{2+} , Zn^{2+} , Cd^{2+} , and Hg^{2+}). *J. Am. Chem. Soc.* **2000**, *122*, 10428–10439.

(50) Chandler, D.; Weeks, J. D.; Andersen, H. C. Van der Waals Picture of Liquids, Solids, and Phase Transformations. *Science* **1983**, *220*, 787–794.

(51) Erickson, R. O. Tubular Packing of Spheres in Biological Fine Structure. *Science* **1973**, *181*, 705–716.

(52) Sharma, A.; Mori, T.; Lee, H.-C.; Worden, M.; Bidwell, E.; Hegmann, T. Detecting, Visualizing, and Measuring Gold Nanoparticle Chirality Using Helical Pitch Measurements in Nematic Liquid Crystal Phases. *ACS Nano* **2014**, *8*, 11966–11976.

(53) Kumar, S. Discotic Liquid Crystal-Nanoparticle Hybrid Systems. *NPG Asia Mater.* **2014**, *6*, e82.

(54) Cha, S.-H.; Hong, J.; McGuffie, M.; Yeom, B.; VanEpps, J. S.; Kotov, N. A. Shape-Dependent Biomimetic Inhibition of Enzyme by Nanoparticles and Their Antibacterial Activity. *ACS Nano* **2015**, *9* (9), 9097–9105.

(55) Suzuki, N.; Wang, Y.; Elvati, P.; Qu, Z.-B.; Kim, K.; Jiang, S.; Baumeister, E.; Lee, J.; Yeom, B.; Bahng, J. H.; Lee, J.; Violi, A.; Kotov, N. A. Chiral Graphene Quantum Dots. *ACS Nano* **2016**, DOI: 10.1021/acs.nano.5b06369.

(56) Kim, Y.; Yeom, B.; Arteaga Barriel, O.; Yoo, S. Y.; Lee, S. G.; Kim, J.-G.; Kotov, N. A. Reconfigurable chiroptical nanocomposites with chirality transfer from the macro- to the nanoscale. *Nat. Mater.* **2016**, DOI: 10.1038/nmat4525.

(57) Chiou, T.-H.; Kleinlogel, S.; Cronin, T.; Caldwell, R.; Loeffler, B.; Siddiqi, A.; Goldizen, A.; Marshal, J. Circular Polarization Vision in a Stomatopod Crustacean. *Curr. Biol.* **2008**, *18* (6), 429–434.